Use of Phalaris canariensis Extract as CO_2 Corrosion Inhibitor of Brass

Jose Gonzalo Gonzalez-Rodriguez *, Edgar Salazar-Salazar, Dante Guillermo Gutierrez- Granda, Earvin Galvan, Ana Karen Larios Galvez, America Maria Ramirez Arteaga, Roy Lopez Cecenes, Alfredo Brito Franco, Jesus Porcayo Calderon

Posted Date: 2 June 2025

doi: 10.20944/preprints202506.0061.v1

Keywords: Brass; Acidic corrosion; green inhibitor; Phalaris canariensis

 doi:10.20944/preprints202506.0061.v1

Article

Use of *Phalaris canariensis* Extract as CO_2 Corrosion Inhibitor of Brass

Edgar Salazar-Salazar [1], Dante Guillermo Gutierrez-Granda [2], Earvin Galvan [2], Ana Karen Larios-Galvez [2], America Maria Ramirez-Arteaga [3], Roy Lopez-Cecenes [3], Alfredo Brito-Franco [2], Jesus Porcayo-Calderon [4] and Jose Gonzalo Gonzalez-Rodriguez [2,*]

[1] Universidad Nacional Autonoma de Mexico, Facultad de Ingeniería, Ciudad Universitaria, Ciudad de Mexico, Mexico
[2] Universidad Autonoma del Estado de Morelos, Centro de Investigacion en Ingenieria y Ciencias Aplicadas, Av. Universidad 1001, Cuernavaca, Mor., Mexico
[3] Universidad Autonoma del Estado de Morelos, Facultad de Ciencias Quimicas e Ingenieria, Av. Universidad 1001, Cuernavaca, Mor., Mexico
[4] Universidad de Sonora, Departamento de Ingeniería Química y Metalurgia, Hermosillo 83000, Sonora, Mexico
* Correspondence: author e-mail: ggonzalez@uaem.mx

Abstract: The corrosion inhibition action of *Phalaris canariensis* extract on brass in a CO_2-saturated 3.5% NaCl solution has been evaluated with the aid of potentiodynamic polarization curves, linear polarization resistance and electrochemical impedance spectroscopy tests. Results have indicated that *Phalaris canariensis* extract is an excellent CO_2 corrosion inhibitor with an efficiency that increases with its concentration, reaching its maximum value of 99% with an inhibitor concentration of 100 ppm, decreasing the corrosion current density for more than two orders of magnitude. The addition of the *Phalaris canariensis* extract increased the pitting potential and decreased the passive current density values and affected cathodic reactions, behaving as a mixed type of inhibitor. The corrosion process was under charge transfer control, and it was neither affected by the addition of the inhibitor nor by elapsing time. Main compounds found in the *Phalaris canariensis* extract included antioxidants such as palmitic and oleic acids.

Keywords: Brass; Acidic corrosion; green inhibitor; *Phalaris canariensis*

1. Introduction

Due to their high corrosion resistance, mechanical properties, electrical and thermal conductivity, copper and its alloys, such as brass, find many applications in the industry, such as drinking water distribution systems, power stations, seawater desalination, submarine and ship construction, pipelines, oil-water separation processes, electronics, etc. Despite the high corrosion resistance of copper and brass, they are susceptible to different types of corrosion when exposed to some environments, especially the selective corrosion of zinc in brass [1-4]. It has been proved that one of the most efficient ways to minimize copper or brass corrosion is by using corrosion inhibitors, especially heterocyclic compounds that contain functional groups with heteroatoms such as nitrogen, oxygen, sulfur and phosphorus, such as amines, azoles, Schiff bases, imidazolines, amides and their derivatives, which can form a layer of protective corrosion products on the metal surface [5-6]. However, these organic compounds are expensive, toxic and harmful to human people and the environment, and thus, a lot of research has been done on the use of more environmentally-friendly corrosion inhibitors [7-20]. Thus, some green inhibitors such as Palm Oil [7, 12], *Aegle marmelos* pulp [8], Shrimp shell waste [9], carbon dots [11], expired ciprofloxacin [13], *Thymus vulgaris* [15], Coffee waste [16], garlic [18] have been evaluated for copper and brass in environments such as atmospheric

 doi:10.20944/preprints202506.0061.v1

[7, 12-14], H_2SO_4 [8], NaCl [9, 10, 16, 19], HCl [14] and H_2NO_3 solutions [17, 18]. However, there is very little information about the CO_2 corrosion of copper or brass [21-23].

In power stations, brass is used in various components like valves, fittings, connectors, and steam condensers due to its resistance to corrosion, especially in water or steam systems. Some pump components, such as impellers and housings, may be made of brass to resist wear and tear, as well as corrosion from fluids like water or oil. In thermal power plants, particularly coal, gas, or oil-fired stations, CO_2 is a byproduct of the combustion of fossil fuels. This CO_2 is present in the flue gases that are emitted during the burning of fuels [24]. While the CO_2 itself is usually not directly mixed with the station working fluids, it may dissolve in water or other fluids used in cooling systems, leading to an increase in CO_2 concentration in these fluids [25]. If the plant uses a wet cooling tower, the flue gases may carry CO_2 into the cooling water, either through direct contact with the air or through leakage from systems like the condenser or scrubbers. When CO_2 dissolves in water, it forms carbonic acid (H_2CO_3), which can lower the pH of the cooling or condensate water [26]. This can lead to corrosion in pipes, heat exchangers, and other parts of the cooling system if not properly controlled. In power stations that use steam turbines, the water in the steam cycle may absorb CO_2 from the combustion gases, especially if the boiler is not fully sealed or if there is any leakage. Over time, CO_2 can build up in the steam and condense back into water within the system [27].

Phalaris canariensis is considered as a pseudo-cereal plant that produces white oval-shaped panicles with green veins, which eventually yield small elliptical seeds of approximately 4 to 5 millimeters in length and 1.5 to 2 millimeters in width. Although it is used mainly as a bird food, it has gained importance for human consumption due to beneficial properties such as antioxidant, antihypertensive and antidiabetic which is because of the presence of amino acids, proteins, minerals and a variety of antioxidants such as flavonoids, vitamin E, fatty acids such as oleic, palmitic and linoleic acids [28-30]. Thus, the aim of this work is to evaluate an environmentally friendly corrosion inhibitor, *Phalaris canariensis*, for the CO_2 corrosion of brass.

2. Experimental Procedure

2.1. Testing Material

Used material in the present research work was commercial brass containing 68.5 (wt. %) Cu-31.5 Zn, in the form of cylindrical bars 6.0 mm in diameter. Specimens measuring 10.0 mm in length were cut and encapsulated in commercial polymeric resin, abraded with 600 grade emerging paper, washed with acetone, and blown with warm air.

2.2. Synthesis of the Inhibitor

For the obtention of the inhibitor, the Soxhlet method was used by using hexane as solvent. For this, *Phalaris canariensis* seeds were crushed, and 400 g of this powder were placed together with 100 ml of hexane in round-bottom flasks, mounted on a heating grill at 68.7 °C, the hexane boiling point temperature, and kept for 24 h. The remaining solvent was evaporated in a rotary evaporator, leaving only the extracted *Phalaris canariensis* oil.

2.3. Working Electrolyte

Working electrolyte consisted of CO_2-saturated 3.5 (wt.%) NaCl solution. For this, a 3.5 % NaCl solution was prepared by using analytical grade reagents. This solution was bubbled during two hours with CO_2 gas, and kept bubbling during the whole test. A three-electrode glass electrochemical cell was used for this purpose, using a Silver/Silver Chloride reference electrode and a 6.0 mm graphite counter electrode. Inhibitor was added to this solution by appropriate dilutions.

2.4. Electrochemical Techniques

 doi:10.20944/preprints202506.0061.v1

Potentiodynamic polarization curves (PPC) and Electrochemical Impedance Spectroscopy tests (EIS) were used to evaluate the inhibitor. Prior to these tests, the Open circuit potential value, OCP, was monitored during 1,800 s. PPC tests were started by polarizing the specimen 700 mV more cathodic than the free corrosion potential value, E_{corr}, scanned into the anodic direction at scan rate of 1 mV/s, and finishing at a potential value of 700 mV more anodic than E_{corr}. Extrapolation of the passivation current density value was used to calculate the corrosion current density value, I_{corr}, since a passive region was found. Inhibitor efficiency value, I.E., was calculated as follows:

$$\text{I.E. } (\%) = (I_{corr1} - I_{corr2})/ I_{corr1} \text{ X } 100 \qquad (1)$$

where ◎corr2 and ◎corr1 are the corrosion current density values with and without inhibitor respectively, whereas the metal fraction covered by the inhibitor,◎◎ was calculated by using:

$$\theta = (I_{corr1} - I_{corr2})/ I_{corr1} \qquad (2)$$

EIS measurements were carried at the E_{corr} value by applying an AC voltage signal of ±10 mV in a frequency range of 100 kHz to 0.01 Hz during 24 h. Morphology of corroded specimens was analyzed in a JEOL JSM-IT500 Scanning Electronic Microscope, SEM, which was coupled to an Oxford energy dispersive spectroscopy, EDS, equipment to carry out semi quantitative chemical analysis of the corrosion products on top of specimens.

3. Results and Discussion

3.1. Chemical Analysis of the Inhibitor

As reported elsewhere [31], chemical composition of *Phalaris canariensis* extract consisted of fatty acids being the most abundant palmitic, oleic, and 17-Octadecynoic acids. Palmitic acid has not double bonds, whereas oleic acid has double bonds in its carbon chain, giving to these compounds antioxidant properties, whereas the former gives more stability to its molecular structure. Double bonds are more chemically reactive than single bonds. It was also reported the presence of C-H bond, as well as the C=O carbonyl group, C-O and C=C bonds. The combination of these functional groups as well as the double bonds, make that these fatty acids can act as corrosion inhibitors. In fact, both Oleic and palmitic acids have been studied as corrosion inhibitors for carbon steel in CO_2 environments [32, 33] and in acidic media [34-36].

3.2. Open Circuit Potential

The effect of the *Phalaris canariensis* extract concentration on the OCP value for brass in the CO_2-saturated 3.5% NaCl solution is depicted in Figure 1, where it can be seen that as the *Phalaris canariensis* extract increases, the OCP value is made nobler. The most active OCP value was for the specimen in the absence of the inhibitor, whereas the noblest value was obtained with the addition of 100 ppm of *Phalaris canariensis* extract. This shift of the OCP value is due to the adsorption of the *Phalaris canariensis* extract to form a protective layer of corrosion products. In the absence of an inhibitor, it has been reported that the main corrosion products formed in brass in aqueous solutions in the presence of CO_2 include the CuO and Cu_2O oxides, $CuCO_3$ and $Cu(OH)_2$ [21, 37] which are very protective, and this is the reason why the OCP value in these conditions is quite stable. When *Phalaris canariensis* extract is added into the solution, this is adsorbed onto the metal surface to form a protective layer, which, in addition to the compounds formed in the absence of the inhibitor, protect in a better way the metal, and the metal surface area covered by this film increases with the inhibitor concentration, shifting the OCP value into the noble direction [22, 23].

 doi:10.20944/preprints202506.0061.v1

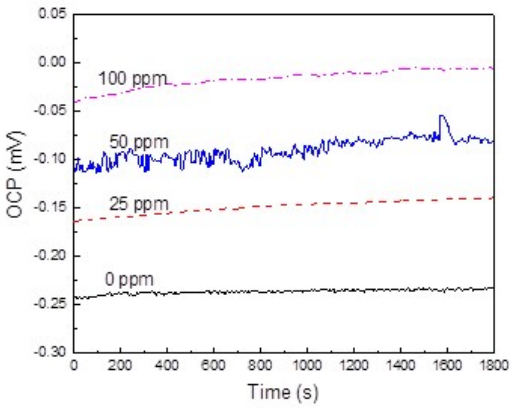

Figure 1. Effect of *Phalaris canariensis* extract concentration on the variation with time of the open circuit potential value, OCP for brass in a CO_2-saturated 3.5% NaCl solution.

3.3. Potentiodynamic Polarization Curves

The effect of the *Phalaris canariensis* extract concentration on the polarization curves for brass in the CO_2-saturated 3.5 % NaCl solution is shown in Figure 2, whereas electrochemical parameters are given in Table 1. It can be observed in Figure 2 that regardless of the inhibitor concentration, data depict behavior. Anodic reactions involve the oxidation of Zn as Zn^{2+} and oxidation of Cu as Cu^{+} and Cu^{2+} as follows:

$$Zn \rightarrow Zn^{2+} + 2e \quad (3)$$

$$Cu \rightarrow Cu^{+} + e \quad (4)$$

$$Cu^{+} \rightarrow Cu^{2+} + e \quad (5)$$

whereas cathodic reaction starts with the dissolution of CO_2 into the liquid phase is the initial step of CO_2 corrosion followed by the formation of carbonic acid (H_2CO_3) by the CO_2 hydration as follows [38]:

$$CO_2 + H_2O \rightarrow H_2CO_3 \quad (6)$$

After this, carbonic acid dissociates to give bicarbonate ion, HCO_3^-, carbonate ion, CO_3^{2-}, and protons, H^+ [39-40].

$$H_2CO_3 \rightarrow H^+ + HCO_3^- \quad (7)$$

$$HCO_3^- \rightarrow H^+ + CO_3^{2-} \quad (8)$$

$$H^+ + e^- \rightarrow \tfrac{1}{2}H_2 \quad (9)$$

In the absence of the inhibitor, two very narrow passive regions are observed at -0.240 and -0.185 mV, whereas a very wide zone which starts at -0.90 mV can be observed. As it was established above, the main corrosion products in the blank, uninhibited solution are CuO and Cu_2O oxides, $CuCO_3$ and $Cu(OH)_2$ [21, 37]. When the inhibitor is added, the passive zone formed by the adsorbed inhibitor onto the metal surface can be still observed, the E_{corr} value is shifted into the noble zone and both the passive and corrosion current density values are decreased as shown in Table 1. The pitting potential value, E_{pit} also moved towards nobler values and the passive current density value decreased as the inhibitor concentration increased. Thus, we can say that the addition of the *Phalaris canariensis* extract improved the passive film properties. It can be seen that the I_{corr} value decreased as the inhibitor concentration increased, obtaining the lowest value with the addition of 100 ppm, which was nearly two orders of magnitude lower than that obtained for the uninhibited solution. Table 1 also shows that the inhibitor efficiency increases as the inhibitor concentration increases, reaching the highest value of 99% with 100 ppm of *Phalaris canariensis* extract. Similarly, the metal fraction covered by the inhibitor, ⊚, also increases with the inhibitor concentration, indicating that the corrosion inhibition is due to the adsorption of the *Phalaris canariensis* extract onto the metal surface area. On the other hand, since there was a passive zone with properties improved by the addition of the inhibitor, no anodic Tafel behavior can be observed, however, cathodic Tafel slope was affected by the addition of the

 doi:10.20944/preprints202506.0061.v1

inhibitor, affecting the cathodic reactions described above, therefore it can be said that *Phalaris canariensis* extract behaves as a mixed type of inhibitor.

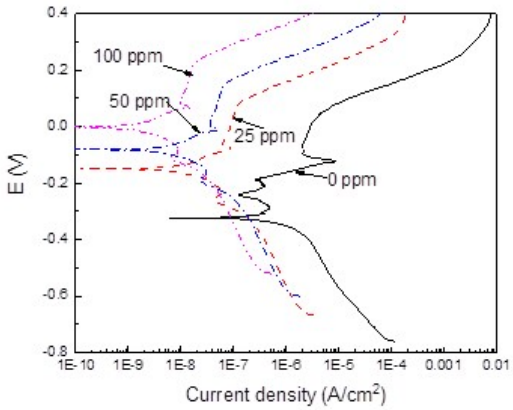

Figure 2. Effect of *Phalaris canariensis* extract concentration on the polarization curves for brass in a CO_2-saturated 3.5% NaCl solution.

Table 1. Electrochemical parameters obtained from potentiodynamic polarization curves.

C_{inh} (ppm)	E_{corr} (V)	I_{corr} A/cm^2)	β_a (V/dec)	β_c (V/dec)	I.E. (%)	θ
0	-0.265	3.7 x 10^{-7}	------	270	-----	---
25	-0.165	6.8 x 10^{-8}	45	520	81	0.81
50	-0.100	3.0 x 10^{-8}	55	540	91	0.91
100	-0.035	1.0 x 10^{-9}	------	555	99	0.99

3.4. Electrochemical Impedance Spectroscopy Tests (EIS)

EIS data in the Nyquist and Bode formats for brass in the CO_2-saturated 3.5% NaCl solution with different concentrations of *Phalaris canariensis* extract is given in Figure 3. Nyquist diagrams, Figure 3 a, display a depressed, capacitive semicircle with its center at the x-axis [3-5] at high and intermediate frequency values, followed by what looks like a second capacitive semicircle at the lowest frequency values, indicating a charge transfer controlled corrosion process [6,7]. The shape of the loops did not change with the inhibitor concentration, indicating that the corrosion mechanism remained unaltered. The high frequency loop represents the electrochemical reactions taking place at the metal-double electrochemical interface, whereas the low frequency loop represents the electrochemical reactions taking place at the metal-corrosion products interface [8-10]. It can be seen that the high frequency loop diameter increases as the inhibitor concentration increases, reaching its highest value at an inhibitor concentration of 100 ppm. On the other hand, Bode format in the impedance format, Figure 3 b, shows that the total impedance increases with the inhibitor concentration, increasing nearly three orders of magnitude with the addition of 100 ppm of inhibitor; two different slopes can be observed in these plots, and thus, the existence of two time constants. The phase angle value increases as the inhibitor concentration increases from around -40 degrees for the uninhibited solution, up to -65 degrees with the addition of 100 ppm of inhibitor, showing a broad peak, indicating the existence of a very protective layer of corrosion products on top of the metal, and the existence of two time constants also.

 doi:10.20944/preprints202506.0061.v1

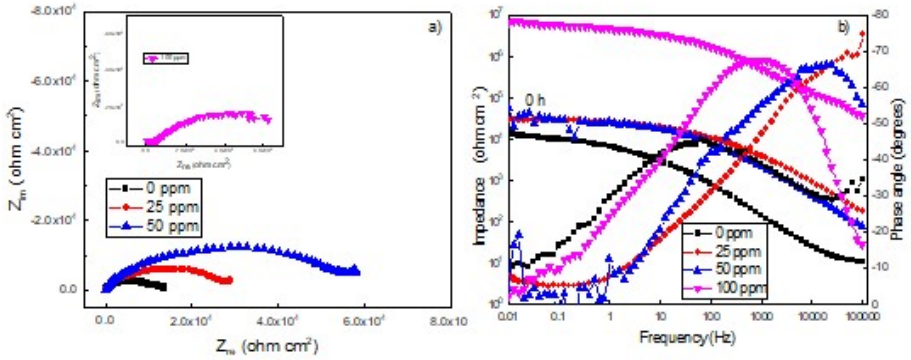

Figure 3. Effect of *Phalaris canariensis* extract concentration on the a) Nyquist and b) Bode plots for brass in a CO_2-saturated 3.5% NaCl solution.

The evolution with time of EIS data for uninhibited solution and the solution containing 100 ppm of inhibitor are shown in Figures 4-5 respectively. For the uninhibited solution, the shape of the Nyquist plots did not change as time elapsed, Figure 4 a, indicating that the corrosion mechanism process was the same with time.

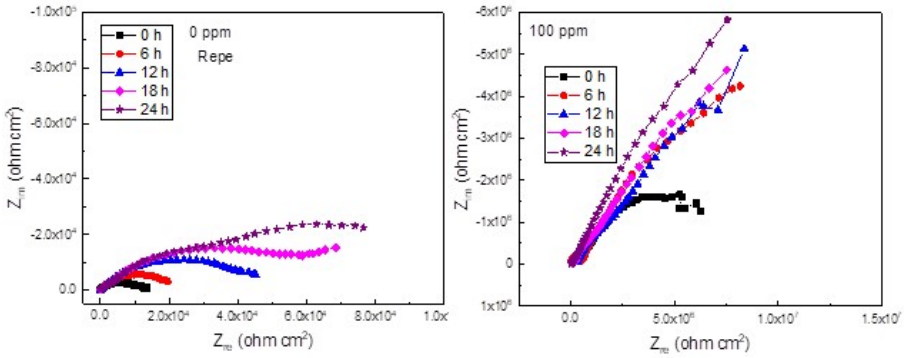

Figure 4. Niquist diagrams for brass in a CO_2-saturated 3.5% NaCl solution containing a) 0 and b) 100 ppm of *Phalaris canariensis* extract.

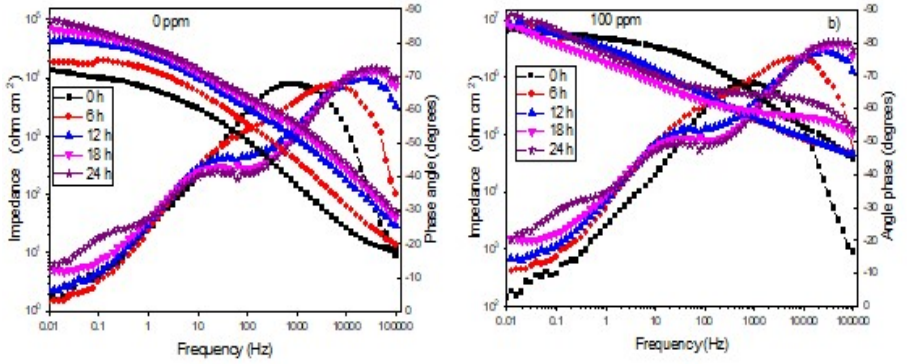

Figure 5. Bode diagrams for brass in a CO_2-saturated 3.5% NaCl solution containing a) 0 and b)100 ppm of *Phalaris canariensis* extract.

The total impedance increased as time elapsed, Figure 4 b, with the existence of two slopes at all testing times, whereas the phase angle increased with time, indicating an increase in the thickness of the protective corrosion products layer, with at least two peaks being observed at all testing times, and thus two different time constants are observed. On the other hand, for the solution containing

 doi:10.20944/preprints202506.0061.v1

100 ppm of inhibitor, Nyquist diagrams was not altered as time elapsed, which means that the corrosion mechanism remained unchanged, Figure 5 b.

Dislike this, the total impedance increased in a slow fashion as time elapsed, and three different slopes are observed for all testing times; on the other side, the phase angle value increased with time, with the existence of three peaks for all testing times, indicating the formation of a very protective corrosion products layer.

EIS data can be simulated by using equivalent electric circuits as those shown in Figure 6. In this figure, R_s represents the electrolyte or solution resistance, R_{ct} the charge transfer resistance, C_{dl} stands for the double electrochemical layer capacitance, R_{ox} stands for the oxide film or any formed corrosion products layer resistance, C_{ox} stands for this oxide capacitance, R_{inh} represents the inhibitor layer resistance and C_{inh} stands for its capacitance. Since the observed loops in Figures 3-5 are depressed due to surface heterogeneities or surface corrosion, ideal capacitances are replaced by a Constant phase element, CPE, which have an impedance, Z_{CPE} given by:

$$Z_{CPE} = Y_0^{-1}(jw)^{-n} \quad (10)$$

where Y_0 is the proportionality constant, j is an imaginary unit, ω is the angular frequency and n is a parameter of the heterogeneity and roughness of the surface [41]. In addition to this, another way to calculate the capacitance of the double electrochemical layer is by using the following expression [42, 43]:

$$C_{dl} = (\varepsilon\varepsilon_0/\lambda)\, A \quad (17)$$

In this expression, ε_0 and ε are the free space permittivity and the dielectric constant of that space respectively, ⌾ the thickness of the double layer and A the electrode surface area.

Obtained electrochemical parameters by using electric circuits shown in Figure 6 are summarized in Tables 2-4. Table 2 shows that as the *Phalaris canariensis* extract increases, the inhibitor efficiency and R_{ct} values increase whereas the CPE_{dl} decreases. In this case, inhibitor efficiency was calculated as follows:

$$\text{I. E. } (\%) = \frac{R_{ct1} - R_{ct2}}{R_{ct1}} \times 100 \quad (18)$$

where R_{ct1} and R_{ct2} denote the charge transfer resistance in the presence and absence of *Phalaris canariensis* extract, respectively. As mentioned earlier, the increase in the inhibitor efficiency is due to the inhibitor adsorption on the brass area forming a protective layer of corrosion products. This decreases in the corrosion rate, as given by the decrease in the I_{corr} value shown in Table 1 brings a decrease in the total number of Cu and Zn ions crossing across the double electrochemical layer bringing, thus, a reduction on the layer conductivity, and therefore, an increase on its resistance represented by R_{ct}. In addition to this the adsorbed *Phalaris canariensis* extract on the brass surface displaces the adsorbed water molecules from the metal, and, since the *Phalaris canariensis* extract molecules are much bigger than the water molecules, the double electrochemical layer thickness value, given by ⌾⌾on Eq. (17), increases, bringing a decreases on the CPE_{dl} value. Table 2 also shows that the inhibitor resistance values, R_{inh}, are bigger than those for R_{ct}, indicating that the formed film by the inhibitor is higher than that for the double electrochemical layer. The increase in the R_{inh} value as the inhibitor concentration is due to a bigger metal surface area covered by the inhibitor and to an increase in the inhibitor-formed film thickness on top of brass. Finally, a value close to 1.0 for parameter n indicates a low metal surface roughness due to a lower metal dissolution rate, whereas values close to 0.5 indicates a high metal surface roughness due to a high corrosion rate. Table 2 shows that for the uninhibited solution, the n_{dl} value is 0.7, indicating a high metal surface roughness because the brass dissolution rate is high. This parameter increases as the inhibitor concentration increases, reaching a maximum value of 0.9 due to a low metal surface roughness because brass has a low corrosion rate under these conditions.

 doi:10.20944/preprints202506.0061.v1

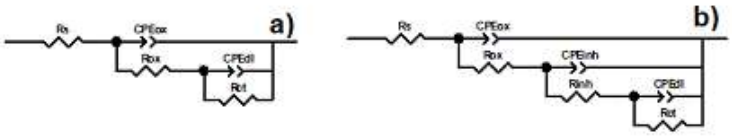

Figure 6. Electric circuits used to simulate the EIS data for brass in a CO_2-saturated 3.5% NaCl+CO_2 solution.

Table 2. Electrochemical parameters used to simulate the EIS data using different *Phalaris canariensis* extract concentrations.

C_{inh} (ppm)	R_{ct} (ohm cm^2)	CPE_{dl} (F cm^{-2})	n_{dl}	R_{ox} (ohm cm^2)	CPE_{ox} (F cm^{-2})	n_{ox}	R_{inh} (ohm cm^2)	$CPEi_{nh}$ (F cm^{-2})	n_{inh}	I.E.(%)
0	1777	4.74×10^{-6}	0.7	10503	6.90×10^{-5}	0.7	------	------	-----	----
25	6959	2.52×10^{-7}	0.8	12079	4.37×10^{-5}	0.8	12489	2.37×10^{-5}	0.8	77
50	12578	1.17×10^{-7}	0.8	18744	2.29×10^{-5}	0.8	36472	1.09×10^{-5}	0.8	88
100	3.6×10^5	6.5×10^{-11}	0.9	6.9×10^6	1.90×10^{-6}	0.9	2.9×10^6	4.8×10^{-6}	0.9	99

Table 3. Electrochemical parameters used to simulate the EIS data for the uninhibited solution.

Immersion time (h)	R_{ct} (ohm cm^2)	CPE_{dl} (F cm^{-2})	n_{dl}	R_{ox} (ohm cm^2)	CPE_{ox} (F cm^{-2})	n_{ox}
0	1777	4.74×10^{-6}	0.7	10503	6.90×10^{-5}	0.7
6	1976	1.3×10^{-6}	0.8	22105	1.3×10^{-5}	0.8
12	2125	8.3×10^{-7}	0.8	46186	8.3×10^{-6}	0.8
18	2468	6.2×10^{-7}	0.9	56360	6.2×10^{-6}	0.9
24	2797	3.7×10^{-7}	0.9	90613	3.7×10^{-6}	0.9

Table 4. Electrochemical parameters used to simulate the EIS data for solution containing 100 ppm of inhibitor.

Immersion time (h)	R_{ct} (ohm cm^2)	CPE_{dl} (F cm^{-2})	n_{dl}	R_{ox} (ohm cm^2)	CPE_{ox} (F cm^{-2})	n_{ox}	R_{inh} (ohm cm^2)	$CPEi_{nh}$ (F cm^{-2})	n_{inh}	I.E .(%)
0	3.6×10^5	6.5×10^{-11}	0.9	6.9×10^6	1.9×10^{-6}	0.9	2.2×10^6	4.8×10^{-6}	0.9	99
6	*4.6×10^5*	*1.6×10^{-7}*	0.5	8.9×10^6	*7.8×10^{-7}*	0.9	*5.2×10^6*	*2.6×10^{-7}*	0.9	99
12	*2.1×10^5*	*1.7×10^{-7}*	0.5	*1.2×10^7*	*4.8×10^{-7}*	0.9	*8.0×10^6*	*1.7×10^{-7}*	0.9	99
18	*1.9×10^5*	*1.1×10^{-7}*	0.6	*1.8×10^7*	*2.9×10^{-7}*	0.9	*1.0×10^7*	*1.4×10^{-7}*	0.9	99
24	*3.7×10^6*	*1.4×10^{-7}*	0.6	*2.7×10^7*	*1.2×10^{-7}*	0.9	*2.4×10^7*	*1.1×10^{-7}*	0.9	99

On the other hand, for uninhibited solution, Table 3, the R_{ct} value did not change very much as the time elapsed unlike the R_{ox} values, which increased as testing time elapsed for almost one order of magnitude, in agreement with the idea that under these conditions, the formed oxides on top of brass brings a decrease on its corrosion rate. However, for the test with the addition of 100 ppm, Table 4, the R_{ct} value increased for almost one order of magnitude and the CPE_{dl} value decreased almost in the same way due to the inhibitor adsorption on the metal surface with a decrease in the metal ions crossing the double electrochemical layer. Additionally, the film-formed inhibitor increases in thickness as testing time elapsed, as evidenced by the increase on the R_{inh} values.

3.5. Surface Characterization

 doi:10.20944/preprints202506.0061.v1

SEM micrographs of corroded specimens in the uninhibited solution and in the presence of 100 ppm of *Phalaris canariensis* extract are shown in Figure 7. For specimen corroded in the uninhibited solution, Figure 7a, surface shows the presence of abrading marks together with numerous, small pits, indicative of the rupture of a passive layer formed on top of the alloy. On the other hand, specimen corroded in the presence of *Phalaris canariensis*, Figure 7 b, the abrading marks are still present, however, the amount of pits is much lower than that in the uninhibited solution, indicative that the passive layer formed on top of the alloy is more protective and less susceptible to be disrupted by aggressive ions present in the electrolyte.

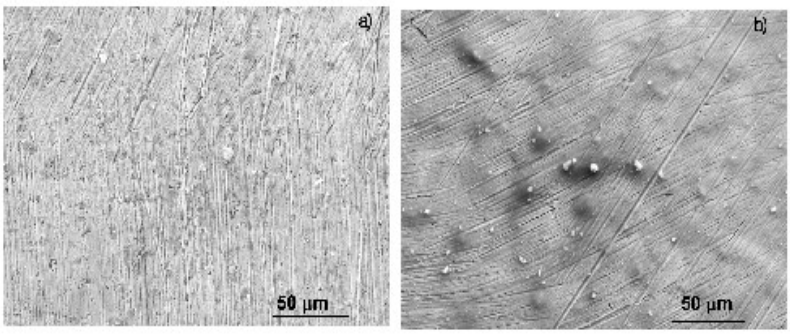

Figure 7. SEM micrographs of brass corroded in a CO_2-saturated 3.5% NaCl+CO_2 solution containing a) 0 and b) 100 ppm of *Phalaris canariensis* extract.

4. Conclusions

A study of *Phalaris canariensis* extract as CO_2-corrosion inhibitor for brass has been carried out. Polarization curves showed that even when in the absence of the inhibitor there is the presence of a passive layer on top of the alloy, however, the passive current density value decreased whereas the pitting potential value increased with the addition of *Phalaris canariensis* extract. For this, and since the cathodic Tafel layer was affected by the inhibitor, therefore, it can be said that *Phalaris canariensis* extract behaves as a mixed type of inhibitor. *Phalaris canariensis* extract was an excellent corrosion inhibitor since its adsorption on to the alloy surface formed a protective passive layer with an efficiency value that increases with increasing its concentration, obtaining a maximum efficiency of 99 % with the addition of 100 ppm of inhibitor. Corrosion mechanism was under charge transfer control and it was not affected neither by the addition of the inhibitor nor by the elapsing time. The adsorption of the inhibitor on to the alloy surface to form a protective passive layer made the charge transfer resistance to increase and the double layer capacitance to decrease. This was due to the existence of antioxidant compounds such as palmitic and oleic acids on the extract.

Author Contributions: Conceptualization and methodology, E.S-S. and D.G.G.-G; software and validation E. G. and A.K.L.-G.; formal analysis and investigation Rz.L.-C. and A.B.-F; data curation and funding acquisition J.P.-C. and A.M.R.-A.; writing-original draft preparation and project administration J.G.G.-R.

Data Availability: The data that support the findings of this study are available within the article.

Acknowledgments: The authors of this work would like to acknowledge to Mr. Jose Juan Ramos-Hernandez and Dr. Maura Casales Diaz for their SEM work.

Competing Interests: The authors declare to have no conflict of interest.

 doi:10.20944/preprints202506.0061.v1

References

1. Yan, H.; Rashid, M.R.B.A.; Khew, S.Y.; Li, F.; Hong, M. Wettability transition of laser textured brass surfaces inside different mediums. *Appl. Surf. Sci.* **2018,** 427, 369-375. https://doi.org/10.1016/j.apsusc.2017.08.218
2. Lu, X.; Liu, Y.; Liu, M.; Wang, Z. Corrosion behavior of copper T2 and brass H62 in simulated Nansha marine atmosphere. J. Mater. Sci. Technol. **2019,**35,1831-1839. https://doi.org/10.1016/j.jmst.2019.04.024
3. Chraka, A.; Seddik, N.B.; Raissouni, I.; Kassout, J.; Choukairi, M.; Ezzaki, M.; Zaraali, O.; Belcadi, H. Electrochemical explorations, SEM/EDX analysis, and quantum mechanics/molecular simulations studies of sustainable corrosion inhibitors on the Cu-Zn alloy in 3% NaCl solution. J. Mol. Liq. **2023,** 387, 122715. https://doi.org/10.1016/j.molliq.2023.122715
4. Dimitrijevic, S.P.; Dimitrijevic, S.B.; Koerdt, A.; Ivanovic, A.; Stefanovic, J.; Stankovic, T.; Gerengi, H. Comparison of Corrosion Resistance of Cu and Cu72Zn28 Metals in Apricot Fermentation Liquid. Materials **2025**, 18, 1253. https://doi.org/10.3390/ma18061253
5. Avdeev, Y.G.; Nenasheva, T.A.; Luchkin, A.Y.; Marshakov, A.I.; Kuznetsov, Y.I. Complex InhibitorProtection of Some Steels in Hydrochloric Acid Solutions by 1,2,4-Triazole Derivatives. Materials **2025**, 18, 464. https://doi.org/10.3390/ma18020464
6. Sedik, A.; Athmani, S.; Saoudi, A.; Ferkous, H.; Ribouh, N.; Lerari, D. Experimental and theoretical insights into copper corrosion inhibition by protonated amino-acids. RSC Adv. **2022,** 12, 23718–23735. https:// doi. org/ 10. 1039/ D2RA0 3535A.
7. Barbosa, M.P.S.; Do Nascimento, C.C.F.; Dos Santos, D.D.M.L. Evaluation of Palm Oil Corrosion Inhibition Through Image Analysis in Copper Pipes Used in Air Conditioning Systems. J. Bio. Tribo Corros. **2025,** 11, 40-48. https://doi.org/10.1007/s40735-025-00961-6
8. Sowjanya, B.; Vykuntam, S.; Raj, A. A.; Arava, A.; King, P.; Vangalapati, M.; Myneni, V.R.; Harnessing the potential of *Aegle marmelos* pulp extract for sustainable corrosion inhibition of brass in 1M H_2SO_4: insights from characterization and optimization. Biomass Conv. Bioref. **2024,** 14, 30997–31008. https://doi.org/10.1007/s13399-023-04740-6.
9. Idriss, H.O.; Seddik, N.B.; Achache, M.; Rami, S.; Zarki, Y.; Ennamri, A.; Janoub, F.; Bouchta, D. Shrimp shell waste-modified natural wood and its use as a reservoir of corrosion inhibitor (L-arginine) for brass in 3% NaCl medium: Experimental and theoretical studies. J. Mol. Liq. **2024,** 398, 124330, https://doi.org/10.1016/j.molliq.2024.124330
10. Hailou, H.; Taghzouti, S.; Lahcen, I. A.; Idrissi, M.B.; Touir, R.; Ebn Touhami, M,E.H. New aryl-himachalene benzylamines derivatives as eco-friendly corrosion inhibitors at low concentration for brass 62/38 in 200 ppm NaCl: Experimental, analyses and theoretical approach. J. Mol. Struct. **2025,** 1319,139345.https://doi.org/10.1016/j.molstruc.2024.139345
11. Liao, J.; Chu, Q.; Zhao, S.; Liu, Z.; Zhang, X. Recent advances in carbon dots as powerful ecofriendly corrosion inhibitors for copper and its alloy. Mater. Today Sust. **2024,** 26,100706. https://doi.org/10.1016/j.mtsust.2024.100706
12. Megahed, M.M.; Abd ElRhiem, E.; Atta, W.; Ghany, N.A.; Abdelbar, M. Investigation and evaluation of the efficiency of palm kernel oil extract for corrosion inhibition of brass artifacts. Sci. Rep. **2025**, 15, 4473. https://doi.org/10.1038/s41598-025-88370-0.
13. Montaser, A,A.; El-Mahdy, M.S.; Mahmoud, E.E.E.; Fouda, A.S. Recycling of expired ciprofloxacin in synthetic acid rain (SAR) solution as a green corrosion inhibitor for copper: a theoretical and experimental evaluation. J. Appl. Electrochem. **2024,**54, 439–456. https://doi.org/10.1007/s10800-023-01966-0
14. Bustos Rivera-Bahena, G.; Ramírez-Arteaga, A.M,; Saldarriaga-Noreña, H.A.; Larios-Gálvez, A. K.; González-Rodríguez, J.G. Romero-Aguilar, M.; López-Sesenes, R. Hexane extract of *Persea schiedeana* Ness as green corrosion inhibitor for the brass immersed in 0.5 M HCl. Sci. Rep. **2024,** 14, 6512. https://doi.org/10.1038/s41598-024-56793-w
15. Gonzalez-Rodriguez, J.G.; Gutierrez-Granda, D.G.; Larios-Galvez, A.K. Use of *Thymus vulgaris* Extract as Green Corrosion Inhibitor for Bronze in Acid Rain. J. Bio Tribo Corros. **2022,** 8, 77-83. https://doi.org/10.1007/s40735-022-00676-y

 doi:10.20944/preprints202506.0061.v1

16. Janoub, F.; Chraka, A.; Kassout, J. Innovative Characterization of Coffee Waste Extracts and Their Derivatives as Efficient Ecological Corrosion Inhibitors for Copper Alloy in 3% NaCl: Phytochemical Investigations, Electrochemical Explorations, Morphological Assessment and New Computational Methodology. J. Bio Tribo Corros. **2024,** 10, 95-104 https://doi.org/10.1007/s40735-024-00901-w
17. Fouda, A.S.; El-Dossoki, F.I. Shady. I.A. Adsorption and corrosion inhibition behavior of polyethylene glycol on α-brass alloy in nitric acid solution. Green Chem. Lett. Rev. **2018,** 11, 67-77, DOI: 10.1080/17518253.2018.1438525
18. Raeisi, S.; Yousefpour, M. The electrochemical study of the garlic extract as a corrosion inhibitor for brass in the nitric acid solution. .Mater. Chem. Phys. **2024.** 312, 128516. https://doi.org/10.1016/j.matchemphys.2023.128516
19. Radovanović, M.B. Tasić, Ž.Z.; Petrović, M.B.; Simonović, A.T.; Antonijević, M.M. Electrochemical and DFT studies of brass corrosion inhibition in 3% NaCl in the presence of environmentally friendly compounds. Sci. Rep. **2019**, 9, 16081, https://doi.org/10.1038/s41598-019-52635-2
20. Vanangamudi, A.; Punniyakoti, S. Cocos nucifera-mediated electrochemical synthesis and coating of CuO/ZnO nanostructures on Fe ship strips for marine application. Green Chem. Lett. Rev. **2024,** 17,2356612 https://doi.org/10.1080/17518253.2024.2356612
21. Feng, B.; Zha, F.; Lid, L.; Wei, J.; Liu, K, The Corrosion Behavior of T2 Brass, in Power Plant Generator Stator Cooling Water. Russ. J. Electrochem. **2019,** 55, 943–952.
22. Vigdorovich, V.I.; Tsygankova, L.E.; Dorohova.; A.N.; Dorohov, A.V. Knyazeva, L.G.; Uryadnikov, A.A. Protective ability of volatile inhibitors of IFKhAN series in atmospheric corrosion of brass and copper at high concentrations of CO_2, NH_3 and H_2S in air. Int. J. Corros. Scale Inhib. **2018,** 7, 331–339.
23. Vigdorovich, V.I. Knyazeva, L.G.; Zazulya, A.N; Prokhorenkov, V.D.; Dorokhov, A.V.; Kuznetsova, E.G.; Uryadnikov, A.A. Goncharova, O.A. Suppression of Atmospheric Corrosion of Brass Using Volatile Inhibitors. Russ. Agric. Sci. **2017,**43, 342–346.
24. Svoboda, R.; Plamer, D.A. Behavior of copper in generator stator cooling-water systems. Power Plant Chem. **2009,** 11, 70–76.
25. Duffeau, F.; Aspden, D.; Coetzee, G. Guide on stator water chemistry management. Study Comm. **2010,** 4, 37–41.
26. Pedersen, K.; Pilarczyk, M.; Quinkertz, R.; Glos, S.; Kuhn, M. Optimization of a CO_2-Free Offshore Power Plant Using Supercritical CO_2. *Proceedings of the ASME Turbo Expo 2024: Turbomachinery Technical Conference and Exposition. Volume 11: Supercritical CO_2*. London, United Kingdom. June 2024, 24–28. V011T28A028. ASME. https://doi.org/10.1115/GT2024-127613
27. Guo, H.; Xu, H.; Xu, C.; Xin, T. Off-design performance analysis and comparison of a coal-based semi-closed supercritical CO_2 cycle under different operational strategies. Energy, **2025,** 315, 134441. https://doi.org/10.1016/j.energy.2025.134441.
28. Abdel-Aal, E.S.M.; Hucl, P.J.; Sosulski, F.W.J. Structural and compositional characteristics of canaryseed （Phalaris canariensis L.). Agric. Food Chem. **1997,**45,3049-3055. doi: 10.1021/jf970100x
29. May, W.E.; Train, J.C.; Greidanus, L. Response of annual canarygrass（Phalaris canariensis L.）to nitrogen fertilizer and fungicide applications. Can. J. Plant Sci. **2022,**102, 83-94. doi: 10.1139/cjps-2020-0221
30. Perera, S.P.; Hucl, P.; L'Hocine, L.; Nickerson, M.T. Microstructure and distribution of oil, protein, and starch in different compartments of canaryseed（Phalaris canariensis L.) Cereal Chem. **2021,** 98,405-422. doi: 10.1002/cche.10381
31. Galvan E, Larios Galvez A K, Ramirez Arteaga A M, Lopez Sesenes R, Gonzalez Rodriguez J G (2024) Electrochemical, gravimetric and surface studies of *Phalaris canariensis* oil extract as corrosion inhibitor for 316 L type stainless steel in H_2O-LiCl mixtures. Sci Rep 14:23370. https://doi.org/10.1038/s41598-024-75423-z
32. Borko, T.; Bilic, G.; Žbulj, K.; Otmacic, J.; Curkovic, H. Individual and Joint Effect of Oleic Acid Imidazoline and $CeCl_3$ on Carbon Steel Corrosion in CO_2-Saturated Brine Solution. *Coatings* **2025,**15,93-102 https://doi.org/ 10.3390/coatings15010093
33. Al-Sabagh, A.M.; Migahed, M.A.; Mishrif, M.R.; Abd-Elraouf, M.; Abd-El-Bary, H.M.; Mohamed, Z.M.; Hussein, B.M. Corrosion Inhibition Efficiency Of Oleic Acid Surfactant Derivatives For Carbon Steel

 doi:10.20944/preprints202506.0061.v1

Pipelines In Petroleum Formation Water Saturated with CO_2. Paper presented at the Offshore Mediterranean Conference and Exhibition, Ravenna, Italy, March **2013**.

34. Fayyad, E.M.; Sadasivuni, K.K.; Ponnamma, D.; Al-Maadeed, M.A.A.; Oleic acid-grafted chitosan/graphene oxide composite coating for corrosion protection of carbon steel. *Carbohydrate Polymers* **2016,**151, 871-878, https://doi.org/10.1016/j.carbpol.2016.06.001.
35. Al-Edan, A.K.; Isahak, W.N.R.W.; Ramli, Z.A.C; Al-Azzawi, W.K.A.; Kadhum, A.A.H.; Jabbar, H.S.; Al-Amiery, A. Palmitic acid-based amide as a corrosion inhibitor for mild steel in 1M HCl. *Heliyon* **2023,**9, 14657. https://doi.org/10.1016/j.heliyon.2023.e14657.
36. Tripathy, D.B.; Murmu, M.; Banerjee, P.; Quraishi, M.A. Palmitic acid based environmentally benign corrosion inhibiting formulation useful during acid cleansing process in MSF desalination plants. *Desalination* **2019,**472, 114128.https://doi.org/10.1016/j.desal.2019.114128.
37. Zhao, H.R.; Xu, Y.L.; Chen, C.K.; Chen, Y.; Liu, Y.W.; Yang, Z.N. New Aspects of Copper Corrosion in a Neutral NaCl Solution in the Presence of Benzotriazole. *Corrosion* **2018,**74, 613-622, https://doi.org/10.5006/2569
38. Bian, C.; Ming, Z.; Han, X. Electrochemical response of mild steel in ferrous ion enriched and CO_2 saturated solutions. *Corros Sci* **2015,**96, 42-58. https://doi.org/10.1016/j.corsci.2015.03.015
39. Paolinelli, L.D.; Perez, T.; Simison, S.N. The effect of pre-corrosion and steel microstructure on inhibitor performance in CO_2 corrosion. Corr Sci 103:2456-2560. Paolinelli LD, Perez T, Simison SN (2008) The effect of pre-corrosion and steel microstructure on inhibitor performance in CO_2 corrosion. *Corr Sci* **2008,**103, 2456-2560. https://doi.org/10.1016/j.corsci.2008.06.031
40. Jia, Z.; Li, X.; Du, C. Effect of acetic acid on CO_2 corrosion of 3Crlow-alloy steel. *Mater Chem Phys* **2012,** 132, 258-271. https://doi.org/10.1016/j.matchemphys.2011.08.034
41. Onyeachu, I.B.; Obot, I.B.; Sorour, A.A.; Abdul-Rashid, M.I. Green corrosion inhibitor for oilfield application I: Electrochemical assessment of 2-(2-pyridyl) benzimidazole for API X60 steel under sweet environment in NACE brine ID196. *Corros Sci* **2019,** 150, 183–193. https://doi.org/10.1016/j.corsci.2019.02.010
42. Karfa, R.P.; Adhikari, U.; Sukul, D. Corrosion inhibition of mild steel in acidic medium by polyacrylamide grafted Guar gum with various grafting percentage: Effect of intramolecular synergism. *Corros Sci* **2014,** 88, 246–253. https://doi.org/10.1016/j.corsci.2014.07.039
43. Bustamante, R.A.; Silve, G.N.; Quijano, M.A.; Hernandez, H.H.; Romo, M.R.; Cuan, A.; Pardave, M.P. Electrochemical study of 2-mercaptoimidazole as a novel corrosion inhibitor for steels. *Electrochim Acta* **2009,**54, 5393–5599. https://doi.org/10.1016/j.electacta.2009.04.029